

Zero-field skyrmions in FeGe thin films stabilized through attaching a perpendicularly magnetized single-domain Ni layer

Zi-Bo Zhang(张子博) and Yong Hu(胡勇)

Citation: Chin. Phys. B, 2021, 30 (**7**): 077503. DOI: 10.1088/1674-1056/abf4bc
Journal homepage: http://cpb.iphy.ac.cn; http://iopscience.iop.org/cpb

What follows is a list of articles you may be interested in

Emergent O(4) symmetry at the phase transition from plaquette-singlet to antiferromagnetic order in quasi-two-dimensional quantum magnets

Guangyu Sun(孙光宇), Nvsen Ma(马女森), Bowen Zhao(赵博文), Anders W. Sandvik, and Zi Yang Meng(孟子杨)
Chin. Phys. B, 2021, 30 (**6**): 067505. DOI: 10.1088/1674-1056/abf3b8

Tunable deconfined quantum criticality and interplay of different valence-bond solid phases

Bowen Zhao(赵博文), Jun Takahashi, Anders W. Sandvik
Chin. Phys. B, 2020, 29 (**5**): 057506. DOI: 10.1088/1674-1056/ab889b

Role of the spin anisotropy of the interchain interaction in weakly coupled antiferromagnetic Heisenberg chains

Yuchen Fan(樊宇辰), Rong Yu(俞榕)
Chin. Phys. B, 2020, 29 (**5**): 057505. DOI: 10.1088/1674-1056/ab820b

Magnetic properties of the double perovskite compound Sr_2YRuO_6

N. EL Mekkaoui, S. Idrissi, S. Mtougui, I. EL Housni, R. Khalladi, S. Ziti, H. Labrim, L. Bahmad
Chin. Phys. B, 2019, 28 (**9**): 097503. DOI: 10.1088/1674-1056/ab3441

Temperature-dependent interlayer exchange coupling strength in synthetic antiferromagnetic$[Pt/Co]_2/Ru/[Co/Pt]_4$ multilayers

Yong Li(李勇), Xiangjun Jin(金香君), Pengfei Pan(潘鹏飞), Fu Nan Tan, Wen Siang Lew, Fusheng Ma(马付胜)
Chin. Phys. B, 2018, 27 (**12**): 127502. DOI: 10.1088/1674-1056/27/12/127502

Zero-field skyrmions in FeGe thin films stabilized through attaching a perpendicularly magnetized single-domain Ni layer*

Zi-Bo Zhang(张子博)[1] and Yong Hu(胡勇)[1,2,†]

[1] Department of Physics, College of Sciences, Northeastern University, Shenyang 110819, China
[2] State Key Laboratory of Rolling and Automation, Northeastern University, Shenyang 110819, China

(Received 27 February 2021; revised manuscript received 23 March 2021; accepted manuscript online 5 April 2021)

A numerical study reports that the zero-field skyrmions in FeGe thin films are stabilized when a FeGe layer is exchange coupled to a single-domain Ni layer, which has been magnetized perpendicularly. Due to the small thickness, an easy-plane anisotropy in the FeGe layer is taken into account, and the skyrmion-crystal state is favored to appear for low anisotropies and intermediate FeGe/Ni interlayer exchange couplings, and finally transformed from a labyrinth-like and into an out-of-plane uniform state for the large couplings or into an in-plane state for the high anisotropies. Furthermore, the maximum skyrmion charge number is bigger for the periodic and fixed boundary conditions with an out-of-plane magnetization; on the contrary, the Bloch-type skyrmions can be frozen and stabilized for the larger couplings on the fixed boundary with an in-plane magnetization, similar to the experimental results of the magnetic-field-induced skyrmions. Finally, the skyrmion charge number and diameter both decrease if the nonmagnetic defects exist, and the skyrmion centers are prone to being captured by defect sites. This work evidences that the ensembles of homochiral skyrmions stabilized in the multilayers fabricated by well-established technologies present a roadmap to design new classes of the materials that can host skyrmions.

Keywords: FeGe thin film, zero-field skyrmion, interlayer exchange coupling, Monte Carlo simulation

PACS: 75.70.Ak, 75.10.Hk, 75.40.Mg **DOI:** 10.1088/1674-1056/abf4bc

1. Introduction

Magnetic skyrmions[1–5] are particle-like magnetic configurations that are easily moved by small electrical currents,[6] and are remarkably robust against defects because of their topology.[7] In other words, thanks to the unique spin topology of skyrmions, which allows them to avoid pinning potentials created by structural imperfections, the depinning current density of magnetic skyrmions in magnetic crystals could be four to five orders of magnitude smaller than that for driving domain walls. Magnetic skyrmions are thus envisioned as information carriers for future nonvolatile, low power consumption, high-density spintronic memory and logic computing devices.[8] Magnetic skyrmions were commonly identified in non-centrosymmetric bulk crystals, e.g., MnSi,[1] FeGe,[9] FeCoSi,[10] and their thin-film counterparts,[11–13] as well as in ultrathin magnetic films epitaxially grown on heavy metals.[14,15] It has been found that the generation and stabilization of magnetic skyrmions usually result from a combination of ferromagnetic exchange and Dzyaloshinskii–Moriya interactions (DMI) in the presence of controllable external stimuli such as magnetic field,[1,12,13] spin-polarized electric current,[16,17] local electric field,[18] and laser,[19] with the first two coupling terms giving rise to a spin helix ground state and the last term breaking the symmetry of "up" and "down" domains in spin spirals. On the other hand, the zero-field skyrmions can effectively reduce the engineering difficulty and energy consumption of devices, and there have been comparably few approaches to be presented for stabilizing skyrmions under zero or lower fields, such as interface engineering,[20–22] magnetic history control,[23] geometrical confinement and edge effect,[24–32] and nano-scale defect fabrication.[33–40]

Chen *et al.*[20] designed a perpendicularly anisotropic Cu/Ni/Cu(001) structure underneath Fe/Ni films to trigger a room-temperature skyrmion ground state through interlayer direct exchange coupling. By using the spin polarized low-energy electron microscopy (SPLEEM), they suggested that the magnitude of interlayer exchange field can be tailored by tuning the thickness of Cu spacer layer. In the next year, Nandy *et al.*[21] further verified this concept on the basis of a first-principle model for a Mn monolayer on a W(001) substrate. They found that the Mn/W_m/Co_n/Pt/W(001) multilayers, with $m = 5$ and 6 spacer layers of W and $n = 4$ reference layers of Co, are the best candidates for generating a sufficiently effective interlayer exchange field to fully substitute the required magnetic field for skyrmion formation. Recently, Sui *et al.*[22] further demonstrated the roles of interfacial coordination number and magnetic state of achiral layer on skyrmion formation under zero field using Monte Carlo techniques.

*Project supported by the National Natural Science Foundation of China (Grant No. 11774045), the Joint Research Fund Liaoning-Shenyang National Laboratory for Materials Science (Grant No. 20180510008), and the Fundamental Research Funds for Central Universities, China (Grant No. N182410008-1).

†Corresponding author. E-mail: huyong@mail.neu.edu.cn

© 2021 Chinese Physical Society and IOP Publishing Ltd

Structurally, Cortés-Ortuño *et al.*[25] discussed the effects of a free boundary and a ferromagnetic rim on magnetic phases such as skyrmion and target states in confined geometries. Du *et al.*[31] found that the helical ground states with distorted edge spins firstly evolved into individual skyrmions due to the edge effect. Zhou and Ezawa[32] presented a conversion between a skyrmion and a domain-wall pair by connecting wide and narrow nanowires. Fallon *et al.*[33] developed a method of nucleating skyrmions with nanoscale defect sites. Similarly, the stability of a skyrmion lattice was highly enhanced in the presence of Mn deficiencies.[34] Using Monte Carlo techniques, Silva *et al.*[35] presented that the effect of pointlike nonmagnetic impurities is somewhat similar to the thermal effect, which encourages the phase transition from a helical to a skyrmion or a bimeron state. Therefore, it has been found that the defects in a clean bulk/surface favor to stabilize skyrmions,[36–40] while what will happen for the topologically protected skyrmion crystals induced by an interlayer exchange coupling if the pointlike nonmagnetic impurities are randomly distributed should be elucidated. In this work, the ensembles of densely arranged skyrmions, probably with a large size dispersion, are stabilized in FeGe thin films under zero field through attaching an achiral Ni magnetic layer, and the roles of boundary conditions and pointlike nonmagnetic defects played on skyrmion crystals are also studied.

2. Model and Monte Carlo method

A FeGe thin film is simulated by two-dimensional (2D) spin arrays lying in the xy plane, where the 100×100 spins placed on the triangular lattice experience an easy-plane magnetic anisotropy due to the small thickness, and couple to each other by direct ferromagnetic exchange interaction and DMI. The central results of simulation are obtained by using periodic boundary conditions (PBC) in the film plane, while the results presented from the open (OBC) and fixed boundary conditions (FBC) are also discussed later. The dipolar interactions are not taken into account.[21] The reason is that, in one aspect, the role of dipolar interactions in the film plane is analogous to an anisotropy that favors spins lying flat,[41] so that the anisotropy can be regarded as an effective constant involving magnetocrystalline and shape contributions. In the film normal, in the other aspect, this approximation is justified by the fact that we are interested in ultrathin films with only one or several monolayers, where the dipolar coupling becomes localized in the zero-thickness limit,[42] similar to the one-monolayer film model adopted by Cortés-Ortuño *et al.*[25] Furthermore, a Ni magnetic layer with the 100×100 spins pointing to the positive z-direction is placed underneath the FeGe layer, providing an out-of-plane interlayer exchange field. This additive layer is single-domain with large out-of-plane anisotropies and perpendicularly magnetized, referring to the single-domain Ni layer sandwiched by Cu fabricated by Chen *et al.*[20] or the single-domain Co multilayers calculated by Nandy *et al.*[21] Vousden *et al.*[43] have numerically studied the skyrmion formation in thin films with an easy-plane magnetic anisotropy, and confirmed that there are still Bloch-type skyrmions to appear. Therefore, for the DMI, we use the bulk term in the FeGe layer.

The Hamiltonian of the FeGe layer can be written as

$$\begin{aligned}\mathcal{H} = & -Ja \sum_{\langle ij\in \mathrm{FeGe}\rangle} \boldsymbol{S}_i \cdot \boldsymbol{S}_j - J'a \sum_{\langle i\in \mathrm{FeGe},\ k\in \mathrm{Ni}\rangle} \boldsymbol{S}_i \cdot \boldsymbol{S}_k \\ & -Da \sum_{\langle i,j\in \mathrm{FeGe}\rangle} r_{ij} \cdot (\boldsymbol{S}_i \times \boldsymbol{S}_j) - Ka^3 \sum_{i\in \mathrm{FeGe}} (\boldsymbol{S}_i^z)^2, \quad (1)\end{aligned}$$

where $\boldsymbol{S}$ is the spin unit vector, $r_{ij} = a\hat{r}_{ij}$ is the position vector pointing from site i to j, and the angular brackets denote the summation over the nearest-neighboring pairs. The magnetic parameters of FeGe used in this paper refer to those estimated by Beg *et al.*[44] In the cubic B20 FeGe helimagnet, the value of saturation magnetization $M_S = 3.84 \times 10^5$ A/m is obtained from the crystal lattice constant and the local magnetic moments of iron and germanium atoms.[45–47] The exchange stiffness parameter value $J = 8.78 \times 10^{-12}$ J/m in the first term of Eq. (1) is calculated based on the Landé g-factor $g = 2$ and the spin-wave stiffness where the FeGe ordering temperature is $T_C = 278.7$ K.[48–50] Furthermore, the long-range FeGe helical period (70 nm) and J can be used to determine the DMI constant $D = 1.58 \times 10^{-3}$ J/m^2 in the third term of Eq. (1). The interlayer exchange stiffness parameter value J' in the second term of Eq. (1) can vary from 0 to 11.414×10^{-12} J/m ($1.3J$), which is possible to be realized by tuning the thickness of the spacer layer, such as the copper spacer layer in Chen *et al.*[20] On the other hand, the easy-plane anisotropy constant K in the last term of Eq. (1) is also changeable from 0 to -2.85×10^6 J/m^3. Both J' and K determine the phase diagrams involving skyrmions. Finally, the nearest-neighboring center-to-center distances of magnetic moments are set by $a = 2$ nm, which is much larger than the atomic lattice constants of FeGe due to the scaling approach for reducing the model size to meet the present standard computational facilities.[51,52]

The initial magnetic state in the FeGe layer is disordered. In order to find the magnetic ground state or the minimum energy state at finite temperatures, we employ the Monte Carlo technique based on a simulated annealing algorithm,[53] which incorporates thermal fluctuations in a nonperturbative manner. The FeGe layer is zero-field-cooled from room temperature, where the FeGe layer is paramagnetic while the Ni layer is ferromagnetic, down to 12 K. The simulation time is measured by Monte Carlo step, in which the 10^4 spins are calculated once. At each temperature, the 10^5 Monte Carlo steps are performed for thermalization and then discarded, followed by another 10^5 Monte Carlo steps to average microscopic spin

configurations. This method has proven to be valid for simulations of the creation and annihilation of skyrmions under the excitation of an external magnetic field[54,55] as well as the magnetic relaxation to ground state in the self-assembly process of magnetic nanoparticles.[41]

3. Results and discussion

After annealing the single FeGe layer, i.e., $J' = 0$, most of the spins are lying in the film plane with $M_Z \sim 0$ and some sites and belts with $M_Z \neq 0$ emerge. On the contrary, in the FeGe layer coupled to a Ni layer with $J' = 8.78 \times 10^{-12}$ J/m, a number of roughly circular-shaped domains with significant size dispersions are formed and densely arranged, separated by the $M_Z = 1$ domain-walls of $\sim$4–6 nm width. We define the size dispersion as different sizes of circular-shaped domains in a configuration. In each circular-shaped domain, the spins rotate progressively with a fixed chirality from the up direction at one edge to the down direction at the center, and then to the up direction again at the other edge. In the perimeter regions, the magnetization vector points perpendicularly to the domain center and the perimeters are thus vortex-like magnetic textures. In the following, all the discernible roughly circular-shaped domains in Fig. 1(b) and the representative magnetic sites in Fig. 1(c) are numbered as Nos. 1–17 and 18–19, respectively; we define θ as an angle between magnetization and the positive z-direction, and study its variation along the x-axis across the domain center in each numbered domain, with the results presented in Fig. 2(a).

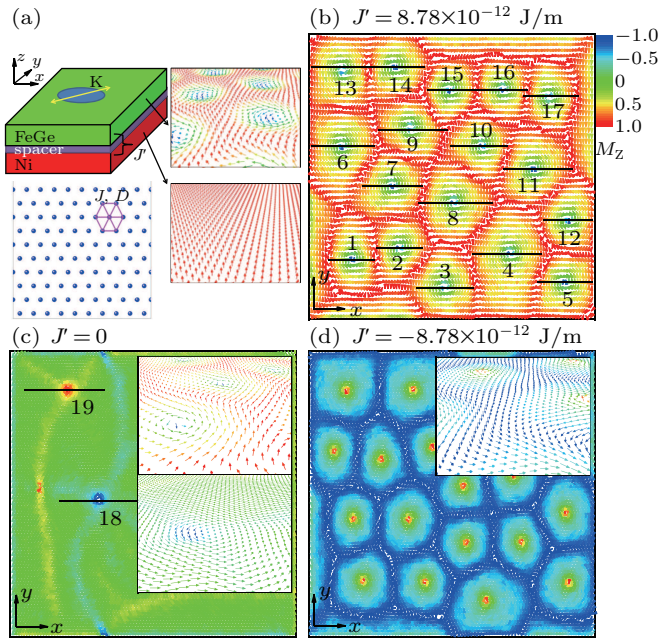


Fig. 1. (a) Schematic illustration of the FeGe/spacer/Ni multilayers where triangular lattice structure, easy-plane magnetic anisotropy (K), intralayer (J) and interlayer exchange couplings (J'), and Dzyaloshinskii–Moriya interactions (D) are shown. (b)–(d) The microscopic spin configurations of the FeGe layer for $J' = \pm 8.78 \times 10^{-12}$ J/m and 0. Insets give the zoomed-in three-dimensional (3D) views. Arrows give the spin orientations and the colors from red to blue represent the spins oriented from the positive to the negative z-direction. Short lines are numbered to prepare for investigating the profile of roughly circular-shaped domains. The coordinate axis is also labeled in the configurations.

For Nos. 1–17 domains, θ is close to 0 at the edges and a sharp increase occurs around the domain centers towards $\theta = \pi$. The position dependence of θ suggests that the imaged circular-shaped spin-textures may be skyrmions[20] and meanwhile safely excludes them from the common bubbles, where no gradual variation of θ exists, or the chiral bubbles, where the sharp increase in θ should occur near the edges.[3] Chen *et al.*[20] in the top-most Fe/Ni bilayer of the multilayer structure, Fe(2.5)/Ni(2)/Cu(8.4)/Ni(15)/Cu(001), made a pixel-by-pixel measurement of the angle θ between magnetization and the (001) surface normal, as a function of distance from a skyrmion center, and showed how the inclination of the magnetization vector with respect to the surface normal reverses with increasing distance from the center of the skyrmion. As a function of distance from the skyrmion center, the angle θ between magnetization and the surface normal direction (001) increases smoothly in almost linear proportion to distance from π to 0, consistent with the theoretical calculations presented above. On the contrary, for Nos. 18–19 domains, θ is calculated as $\sim (1/2)\pi$ near the edges, and around the domain centers, θ may either increase towards π (No. 18) or decrease towards 0 (No. 19). Hence Nos. 18–19 domains are not skyrmionic. It is interesting that different sized skyrmions stabilized under zero field are densely arranged while they do not form periodically ordered arrays, distinct from the regular hexagonal or square skyrmion crystals[56–58] or the isolated skyrmions randomly distributed in large-area ferromagnetic domains (skyrmion gas).[23] Furthermore, the chirality can be analyzed more quantitatively by measuring the statistical distribution of magnetization directions as a function of location with respect to the domain centers. In other words, in the context of 2D and quasi-2D systems, the topological structure of a spin texture is generally characterized by a topological charge, which can be calculated based on the exact spin texture configuration according to[2]

$$Q = \frac{1}{4\pi} \int \mathrm{d}^2 r \cdot S(r) \cdot (\partial_x S(r) \times \partial_y S(r)). \tag{2}$$

The topological charge basically counts how many times the reduced local magnetization (i.e., the spin) $S(r)$ wraps the 2D surface of a 3D ball in the 3D space as the coordinate (x, y) spans the whole planar space. For one skyrmion, the unit topological charge should be granted. Figure 2(b) gives the results of magnetic phase transition and topological charge number with K and J'. The nonzero Q is obtained in the proper J' and K ranges, labelled by red dots. For the configurations presented in Fig. 1, $|Q|$ is equal to 17 for $J' = 8.78 \times 10^{-12}$ J/m and $K = -1.76 \times 10^6$ J/m^3, while $|Q|$ is equal to 0 for $J' = 0$.

The numbers of circular-shaped domains are consistent with $|Q|$, supporting that the circular-shaped domains numbered by Nos. 1–17 are skyrmions. On the contrary, the spins at the edges of Nos. 18–19 domains lay flat in the film plane, because θ is roughly equal to 0.5π. Nevertheless, Q is equal to 0, which excludes the states of vortex ($Q = -0.5$), meron ($Q = -0.5$) and bimeron ($Q = -1$).[2] Thus the domains of Nos. 18–19 are not topological and only the nucleation sites. In other words, these results confirm that the circular-shaped domains are chiral skyrmions, implying that the interlayer coupling is responsible for the skyrmion formation. Note that in order to avoid the occasionality, the microscopic spin configuration in the FeGe layer coupled to the Ni layer with $J' = -8.78 \times 10^{-12}$ J/m is also calculated, as seen in Fig. 1(d), and clearly, the circular-shaped domains also emerge, while with the opposite chirality, to evidence the role of interlayer coupling. Furthermore, the high topological charge number ($|Q|$ exceeds 50) is identified to appear at the low value of K (-1.1×10^6 J/m^3 to 0) and the intermediate value of J' (1.756×10^{-12} to 4.39×10^{-12} J/m).

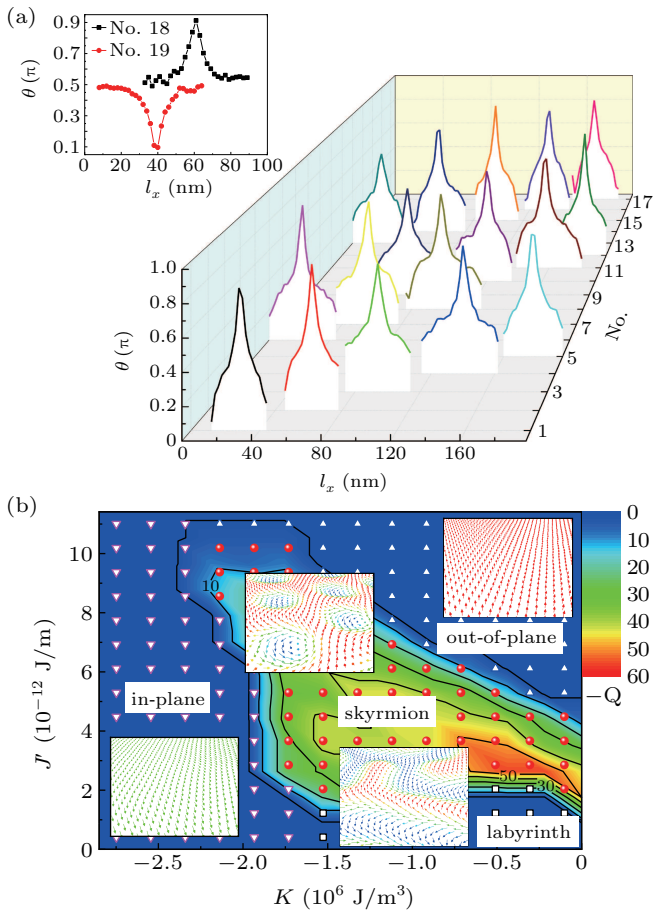


Fig. 2. (a) The angle (θ) between magnetization and the positive z-direction as a function of the spatial position along the x-axis (l_x) in Nos. 1–19 domain, named in Figs. 1(b) and 1(c). (b) The J'–K magnetic phase diagram of the FeGe layer with topological charge number (Q), indicated by the color filled contour. Insets also present the representative microscopic spin configurations where arrows denote the spin orientations and the colors from red to blue denote the spins oriented from the positive to the negative z-direction.

As shown in Fig. 2(b), remarkably, there are several magnetic phase transitions to exist with increasing either K or J'. At the small K and J', a labyrinthlike domain, other than a regularly parallel spin spiral, appears, different from the results obtained by Chen *et al.*[20] and Nandy *et al.*[21], while similar to the initial domain state generated by the static field in a 2 μm Pt/Co/Ta disc.[59] Although the ferromagnetic exchange interaction and the DMI favor a spin spiral domain state, the easy-plane magnetic anisotropy enhances the diversity of degenerate magnetic states to break the periodicity of the spin spiral along a specific direction.[60,61] With further increasing K, the magnetic states transform into in-plane magnetization states, i.e., the spins are lying flat in the film plane. On the contrary, with increasing J' at the small K, the skyrmions are initiated from the corners or the ends of domain belts and a mixed magnetic state replaces the labyrinth states, followed by the dense skyrmion crystals with further increasing J'. When K is small while J' is sufficiently large, the skyrmion crystals may suddenly vanish, giving access to an out-of-plane uniform state. On the other hand, the skyrmion formation may remain at large J' so long as K properly increases. Nevertheless, in these J' and K ranges, the skyrmions may exhibit high size dispersions in a configuration, as shown in Fig. 1(b), or the skyrmions coexist with the out-of-plane uniform state; in other words, the skyrmion crystal gradually transforms into the skyrmion gas. Finally, at large J' and K, the skyrmions annihilate, and the magnetic states go way to either an out-of-plane uniform state at the high J', or to an in-plane magnetization state at large K.

Next, the mechanisms of magnetic phase transitions involving magnetic skyrmion formation are discussed through the energy profile, as shown in Fig. 3. For the in-plane uniform states, the energy results with increasing K are all horizontal lines for different J', and their values are identical, designating that the energy of the configurations with the in-plane uniform state is independent of J' and K. When the FeGe spins lay flat in the film plane, the easy-plane anisotropy energy is constant and minimized. Moreover, since the FeGe spin orientations are perpendicular to those of Ni, J' does not work. The energy of the in-plane uniform state is the lowest when K is large enough, and thus the in-plane magnetization states are stabilized and tend to appear for large K. On the contrary, for the out-of-plane uniform states, the FeGe spin orientation is pointing to one of the hard axes of K, and the easy-plane anisotropy energy is maximized for a given K and increases in a linear proportion to K. As a result, the energy results of the configurations with the out-of-plane uniform state with increasing K are the lines by the same slope. On the other hand, the out-of-plane orientations of the FeGe spins become parallel to those of the Ni spins, resulting in the minimized interlayer exchange energy with a lower value for a larger J'. Therefore,

the large J' favors the emergence of the configurations of the out-of-plane uniform state, in particular at a small K. For the nonuniform states such as labyrinth or skyrmion states, the energies of the configurations are still linearly proportional to K, while the values of J' and K together determine the slope of the lines. For large K, the energies of nonuniform configurations are in between those of in-plane and out-of-plane uniform states. Nevertheless, when K is small, all the energies of configurations are approaching. For $J' = 0$, only the labyrinth states are stable and they will directly transform into the in-plane uniform states with increasing K. With initially increasing J', the energies of the labyrinth and skyrmion states may be nearly overlapped (seen in Fig. 3(b)), and at this point, the labyrinth and skyrmion states may appear in an equal probability. With further increasing J', the skyrmion states at an intermediate K may be more stable, while at no or small K the out-of-plane uniform states may be favored as J' is large enough. In summary, the energy behaviors of different configurations evolved by J' and K effectively interpret the J'–K magnetic phase diagram and demonstrate the formation and annihilation of skyrmion states in the FeGe thin film exchange coupled to a Ni magnetic layer with an out-of-plane uniform magnetization.

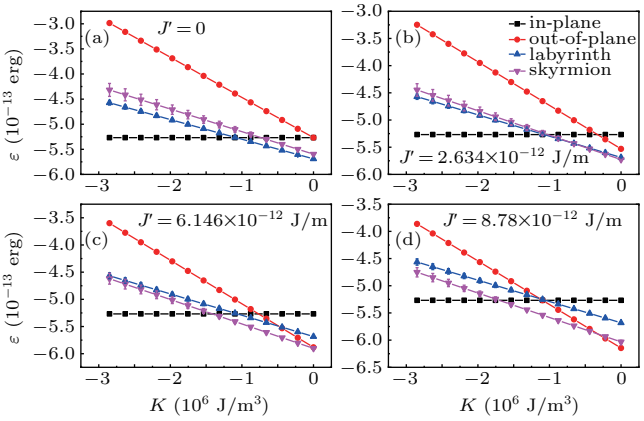


Fig. 3. Energy as a function of K at selected J' for different microscopic spin configurations, where the errors are determined by selecting different labyrinth or skyrmion-crystal configurations.

As mentioned previously, the geometrical confinement and edge effects[24–32] both encourage the stabilization of skyrmions. In the FeGe nanostripes, Du *et al.*[31] observed experimentally that the helical ground states with distorted edge spins evolve into the individual skyrmion states, which develops a way of skyrmion formation through using edge effects. Therefore, the boundary effect of the FeGe/spacer/Ni multilayers on the skyrmion formation is studied. As shown in Fig. 4, the magnetic phase transitions from labyrinth into skyrmion crystal, skyrmion gas, and into uniform states with increasing J' are identical for different boundary conditions. Conversely, the skyrmions do not form near the boundary for the OBC, in contrast to the results obtained for the FBC. Interestingly, the experimental findings driven by magnetic field

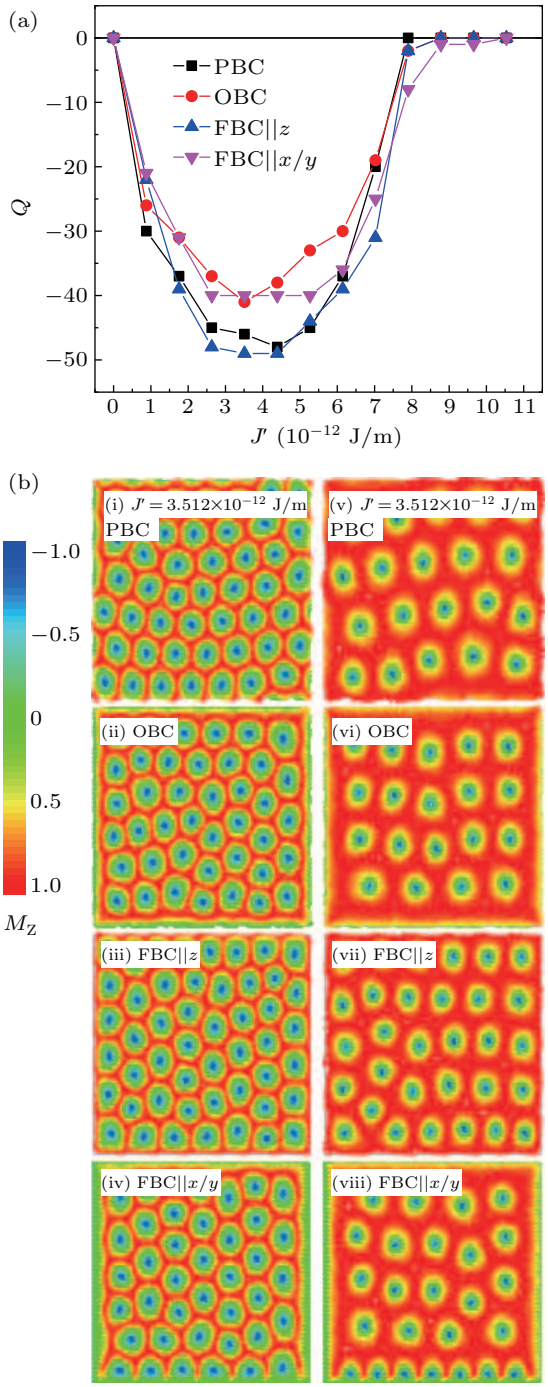


Fig. 4. (a) Topological charge number as a function of J' for different boundary conditions at $K = -1.1 \times 10^6$ J/m^3. (b) Microscopic spin configurations with skyrmion states for (i)–(iv) $J' = 3.512 \times 10^{-12}$ J/m and (v–viii) $J' = 7.024 \times 10^{-12}$ J/m, where arrows give the spin orientations and the colors from red to blue represent the spins oriented from the positive to the negative z-direction. PBC, OBC, FBC||z and FBC||x/y denote periodic boundary conditions, open boundary conditions, and fixed boundary conditions with the magnetization at the edges along the positive-z and positive-x/y directions, respectively.

in the FeGe nanostripes are reproduced by tuning J' for the FBC||x/y, where the skyrmions tend to initially appear at the edges, indicating that the distorted spins at the edges tend to lay flat and be parallel to the edges due to the shape effect.[31] Furthermore, the peak of $|Q|$ with increasing J' appears around the same values of J' for different boundary conditions. However, $|Q|$ may be larger for the PBC and FBC||z, which makes

it acceptable that the FeGe spins at the edges for the PBC and FBC||z favor/fix to point to the positive-z direction, and help J' to break the energy balance between the ferromagnetic exchange coupling and the DMI in the FeGe layer, and then to encourage the stabilization of skyrmions. For large J', the skyrmion-crystal state evolves into the skyrmion-gas state, and remarkably, the annihilation of skyrmions slows down for the FBC, which opens an avenue of controlling skyrmions through manipulating the edge magnetization.

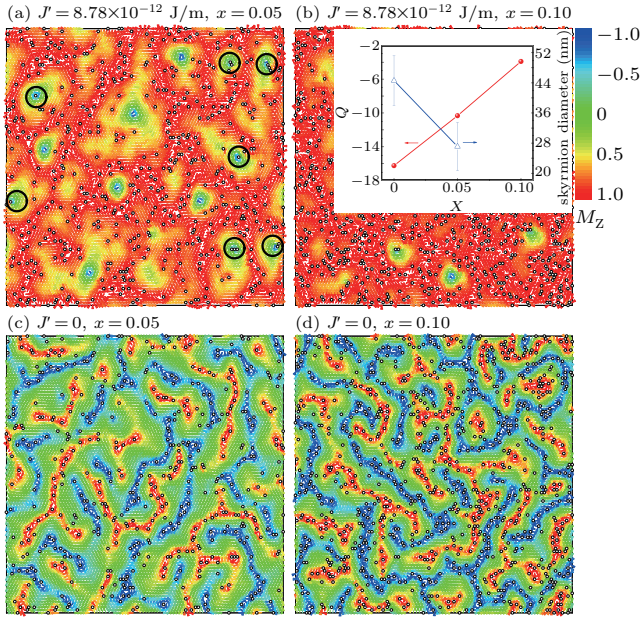


Fig. 5. Microscopic spin configurations of the FeGe layer for the selected J' and x, where the nonmagnetic defect sites are indicated by white dots and arrows give the spin orientations and the colors from red to blue represent the spins oriented from the positive to negative z-direction. The skyrmions captured by defect sites are highlighted by black rings. Inset also gives the results of Q and skyrmion diameter with x, where the errors are determined by measuring different skyrmion sizes in a configuration.

Finally, the influence of nonmagnetic defects with low occupation fractions on the stabilization of skyrmions is studied. Previously, Müller and Rosch in their numerical work[40] have investigated how a single hole defect affects the dynamics of a single skyrmion in a magnetic film. Their hole defect was defined as a vacancy with small radius compared to the skyrmion radius. They found that for high current densities single holes are able to capture moving skyrmions, and they estimated that using a hole with a diameter of 10 nm for a FeGe film with a thickness of 50 nm under a magnetic field of 0.2 T, the impurity-skyrmion potential can provide a sufficiently thermal stability. For the stabilization of magnetic states, Silva *et al.*[35] found that the spins around the hole border tend to lie on the plane, developing a vortex-like configuration, and larger holes may favor bimeron appearance throughout the whole sample, indicating their nonlocal influence. Fig. 5 delineates the results of magnetic states when the pointlike nonmagnetic defects at the occupation fractions of $x = 5\%$ and 10% are randomly, uniformly introduced in the FeGe layer. The nonmagnetic defects are introduced in the initial state, and the locations of the nonmagnetic defect sites do not change during cooling and thus the quenched disorder is considered. It is remarkable that a spin vacancy generates an interaction potential that attracts the skyrmion centers, as the role played by hole defects[35,40] and the influence of spin vacancy on the skyrmion formation is independent of the crystal lattice structure.[33–40]

Furthermore, Silva *et al.*[35] also studied the influence of point-like nonmagnetic impurities with a 5% occupation fraction on the stability of skyrmions. The distribution of these impurities is identical to that adopted above, as shown in Fig. 5. They proposed that the main effects of these pointlike nonmagnetic impurities are somewhat similar to the thermal effect, which is absent for the hole nonmagnetic defects. In other words, the impurities may completely destroy the collective skyrmion sixfold order as well as the individual skyrmions themselves. In the single FeGe layer, the defects induce the in-plane multi-domains around the isolated defect sites or along the defect belts. On the contrary, in the FeGe layer coupled to the Ni layer, the skyrmion states are still observed at $x = 5\%$, with a reduced skyrmion number and a smaller averaged skyrmion size, as shown in the inset of Fig. 5. At $x = 5\%$ and 10%, the topological charge number in the FeGe layer varies from -17 to -11 and -4, respectively, designating that the randomly, uniformly distributed nonmagnetic defects impede the labyrinth states evolving into the skyrmion states. On the other hand, in a skyrmion-crystal configuration, the size difference of skyrmions, i.e., the size dispersion, is as high as up to 16 nm both for $x = 0$ and 5%. Furthermore, the defects suppress the skyrmion grown, and the skyrmions are compressed with the average diameter nearly decreasing to a half at $x = 5\%$. At $x = 10\%$, the skyrmion diameters further shrink and are hardly measured due to too high size dispersions and so many nonmagnetic spin vacancies, although the skyrmions can still be identified through Q. Garanin *et al.*[62] using Monte Carlo simulations studied the thermal creation of skyrmion crystals in a 2D ferromagnetic film with perpendicularly magnetic anisotropy and DMI. At zero temperature, the skyrmions only appear in the magnetization process in the presence of static disorder, while the thermal fluctuations violate the conservation of the topological charge and tend to suppress skyrmions through reducing magnetic anisotropy. Experimental findings[63,64] and theoretical calculations[62] both supported that the elevated temperatures assist the formation of skyrmion structures, and once such a structure is formed, it can be frozen into a regular skyrmion lattice by reducing the temperature. In this paper, the skyrmion crystals are stabilized by balancing different energies such as ferromagnetic exchange interaction, DMI, easy-plane anisotropy and interlayer exchange interaction. Once the pointlike nonmagnetic

defects are introduced, the spin vacancy reduces the interlayer exchange interaction and thus the skyrmions are suppressed. Therefore, it is valid that the role of defects is equivalent to the thermal effect on breaking the skyrmion-crystal structures and suppressing the skyrmions. In other words, the thermal effect on the stabilization of skyrmions in magnetic bilayers under zero field is worth being deeply investigated and thus this will be a work in progress.

4. Conclusion

In summary, based on the Monte Carlo simulation, we found the zero-field skyrmion states stabilized in an easy-plane anisotropic FeGe layer through interlayer coupling to an achiral Ni layer with the spins pointing to the positive z-direction. In the skyrmion ensembles, the skyrmions may be of the great size dispersions and densely arranged, depending on J' and K. Furthermore, the dependence of skyrmions on the boundary conditions and the randomly, uniformly distributed point-like nonmagnetic defects is also studied. The boundary conditions may only change quantitatively, rather than qualitatively, the skyrmion charge number, whereas the topological charge number and the skyrmion size both shrink due to the existence of defects, and the skyrmions captured by the defects are also observed. Precisely controlling the magnetic energies and the lattice structures, which are both responsible for such zero-field skyrmion states in the wide J' and K ranges, provides a pathway to engineer the formation and controllability of skyrmions in exchange-coupled multilayers. The simplicity of magnetic materials and the easily tunable properties make the exchangecoupled chiral/achiral multilayers of interest as a potential test bed for studying the physics of skyrmions under zero field.

Acknowledgment

The authors express their thanks to Dr. Gong Chen for helping with this work, and acknowledge the valuable suggestions from the peer reviewers.

References

[1] Mühlbauer S, Binz B, Jonietz F, Pfleiderer C, Rosch A, Neubauer A, Georgii R and Böni P 2019 *Science* **323** 915
[2] Zhang X, Zhou Y, Song K M, Park T E, Xia J, Ezawa M, Liu X, Zhao W, Zhao G and Woo S 2020 *J. Phys.: Condens. Matter* **32** 143001
[3] Fert A, Reyren N and Cros V 2017 *Nature Rev. Matter.* **2** 17031
[4] Jiang W, Chen G, Liu K, Zang J, te Velthuis S G E and Hoffmann A 2017 *Phys. Rep.* **704** 1
[5] Wiesendanger R 2016 *Nature Rev. Mater.* **1** 16044
[6] Jonietz F, Mühlbauer S, Pfleiderer C, Neubauer A, Münzer W, Bauer A, Adams T, Georgii R, Böni P, Duine R A, Everschor K, Garst M and Rosch A 2010 *Science* **330** 1648
[7] Nagaosa N and Tokura Y 2013 *Nat. Nanotech.* **8** 899
[8] Zhou Y 2019 *Natl. Sci. Rev.* **6** 210
[9] Wilhelm H, Baenitz M, Schmidt M, Rößler U K, Leonov A A and Bogdanov A N 2011 *Phys. Rev. Lett.* **107** 127203
[10] Münzer W, Neubauer A, Adams T, Mühlbauer S, Franz C, Jonietz F, Georgii R, Böni P, Pedersen B, Schmidt M, Rosch A and Pfleiderer C 2010 *Phys. Rev. B* **81** 041203
[11] Tonomura A, Yu X, Yanagisawa K, Matsuda T, Onose Y, Kanazawa N, Park H S and Tokura Y 2012 *Nano Lett.* **12** 1673
[12] Yu X Z, Kanazawa N, Onose Y, Kimoto K, Zhang W Z, Ishiwata S, Matsui Y and Tokura Y 2011 *Nat. Mater.* **10** 106
[13] Yu X Z, Onose Y, Kanazawa N, Park J H, Han J H, Matsui Y, Nagaosa N and Tokura Y 2010 *Nature* **465** 901
[14] Heinze S, von Bergmann K, Menzel M, Brede J, Kubetzka A, Wiesendanger R, Bihlmayer G and Blügel S 2011 *Nat. Phys.* **7** 713
[15] Romming N, Hanneken C, Menzel M, Bickel J E, Wolter B, von Bergmann K, Kubetzka A and Wiesendanger R 2013 *Science* **341** 636
[16] Iwasaki J, Mochizuki M and Nagaosa N 2013 *Nat. Nanotechnol.* **8** 742
[17] Sampaio J, Cros V, Rohart S, Thiaville A and Fert A 2013 *Nat. Nanotechnol.* **8** 839
[18] Seki S, Yu X Z, Ishiwata S and Tokura Y 2012 *Science* **336** 198
[19] Berruto G, Madan I, Murooka Y, Vanacore G M, Pomarico E, Rajeswari J, Lamb R, Huang P, Kruchkov A J, Togawa Y, LaGrange T, McGrouther D, R?nnow H M and Carbone F 2018 *Phys. Rev. Lett.* **120** 117201
[20] Chen G, Mascaraque A, N'Diaye A T and Schmid A K 2015 *Appl. Phys. Lett.* **106** 242404
[21] Nandy A K, Kiselev N S and Blügel S 2016 *Phys. Rev. Lett.* **116** 177202
[22] Sui M X, Zhang Z B, Chi X D, Zhang J Y and Hu Y 2021 *Front. Phys.* **16** 23501
[23] Duong N K, Raju M, Petrović A P, Tomasello R, Finocchio G and Panagopoulos C 2019 *Appl. Phys. Lett.* **114** 072401
[24] Zheng F, Li H, Wang S, Song D, Jin C, Wei W, Kovács A, Zang J, Tian M, Zhang Y, Du H and Dunin-Borkowski R E 2017 *Phys. Rev. Lett.* **119** 197205
[25] Cortés-Ortuño D, Romming N, Beg M, von Bergmann K, Kubetzka A, Hovorka O, Fangohr H and Wiesendanger R 2019 *Phys. Rev. B* **99** 214408
[26] Gilbert D A, Maranville B B, Balk A L, Kirby B J, Fischer P, Pierce D T, Unguris J, Borchers J A and Liu K 2015 *Nat. Commun.* **6** 8462
[27] Sun L, Cao R X, Miao B F, Feng Z, You B, Wu D, Zhang W, Hu A and Ding H F 2013 *Phys. Rev. Lett.* **110** 167201
[28] Liu G B, Li D, de Chatel P F, Wang J, Liu W and Zhang Z D 2016 *Chin. Phys. B* **25** 067203
[29] Jin C M and Du H F 2015 *Chin. Phys. B* **24** 128501
[30] Tang J, Kong L, Wang W, Du H and Tian M 2019 *Chin. Phys. B* **28** 087503
[31] Du H, Che R, Kong L, Zhao X, Jin C, Wang C, Yang J, Ning W, Li R, Jin C, Chen X, Zang J, Zhang Y and Tian M 2015 *Nat. Commun.* **6** 8504
[32] Zhou Y and Ezawa M 2014 *Nat. Commun.* **5** 4652
[33] Fallon K, Hughes S, Zeissler K, Legrand W, Ajejas F, Maccariello D, McFadzean S, Smith W, McGrouther D, Collin S, Reyren N, Cros V, Marrows C H and McVitie S 2020 *Small* **16** 1907450
[34] Ouyang T Y, Shu G J, Hu C D and Chou F C 2014 *IEEE Trans. Magn.* **50** 1500404
[35] Silva R L, Secchin L D, Moura-Melo W A, Pereira A R and Stamps R L 2014 *Phys. Rev. B* **89** 054434
[36] Brown B L, Täuber U C and Pleimling M 2019 *Phys. Rev. B* **100** 024410
[37] Desplat L, Suess D, Kim J V and Stamps R L 2018 *Phys. Rev. B* **98** 134407
[38] Mochizuki M 2017 *Appl. Phys. Lett.* **111** 092403
[39] Hanneken C, Kubetzka A, von Bergmann K and Wiesendanger R 2016 *New J. Phys.* **18** 055009
[40] Müller J and Rosch A 2015 *Phys. Rev. B* **91** 054410
[41] Bian B, Chen G, Zheng Q, Du J, Lu H, Liu J P, Hu Y and Zhang Z 2018 *Small* **14** 1801184
[42] Rohart S and Thiaville A 2013 *Phys. Rev. B* **88** 184422
[43] Vousden M, Albert M, Beg M, Bisotti M A, Carey R, Chernyshenko D, Cortés-Ortuño D, Wang W, Hovorka O, Marrows C H and Fangohr H 2016 *Appl. Phys. Lett.* **108** 132406
[44] Beg M, Carey R, Wang W, Cortés-Ortuño D, Vousden M, Bisotti M A, Albert M, Chernyshenko D, Hovorka O, Stamps R L and Fangohr H 2015 *Sci. Rep.* **5** 17137
[45] Pauling L and Soldate A M 1948 *Acta Cryst.* **1** 212
[46] Richardson M 1967 *Acta Chem. Scand.* **21** 2305

[47] Yamada H, Terao K, Ohta H and Kulatov E 2003 *Physica B* **329–333** 1131
[48] Grigoriev S V, Maleyev S V, Okorokov A I, Chetverikov Y O, Georgii R, Böni P, Lamago D, Eckerlebe H and Pranzas K 2005 *Phys. Rev. B* **72** 134420
[49] Lebech B, Bernhard J and Freltoft T 1989 *J. Phys.: Condens. Matter* **1** 6105
[50] Hamrle J, Gaier O, Min S G, Hillebrands B, Sakuraba Y and Ando Y 2009 *J. Phys. D: Appl. Phys.* **42** 084005
[51] D'Albuquerque e Castro J, Altbir D, Retamal J C and Vargas P 2002 *Phys. Rev. Lett.* **88** 237202
[52] Vargas P, Altbir D and d'Albuquerque e Castro J 2006 *Phys. Rev. B* **73** 092417
[53] Heim B, R?nnow T F, Isakov S V and Troyer M 2015 *Science* **348** 215
[54] Hu Y, Chi X, Li X, Liu Y and Du A 2017 *Sci. Rep.* **7** 16079
[55] Chi X and Hu Y 2018 *Acta Phys. Sin.* **67** 137502 (in Chinese)
[56] Rößler U K, Bogdanov A N and Pfleiderer C 2006 *Nature* **442** 797
[57] Kovrizhin D L, Douc?ot B and Moessner R 2013 *Phys. Rev. Lett.* **110** 186802
[58] Tanigaki T, Shibata K, Kanazawa N, Yu X, Aizawa S, Onose Y, Park H S, Shindo D and Tokura Y 2015 *Nano Lett.* **15** 5438
[59] Woo S, Litzius K, Krüger B, Im M Y, Caretta L, Richter K, Mann M, Krone A, Reeve R M, Weigand M, Agrawal P, Lemesh I, Mawass M A, Fischer P, Kläui M and Beach G S D 2016 *Nat. Mater.* **15** 501
[60] Moon K W, Yoon J, Kim C and Hwang C 2017 *Phys. Rev. Appl.* **12** 064054
[61] Kuchkin V M and Kiselev N S 2020 *Phys. Rev. B* **101** 064408
[62] Garanin D A, Chudnovsky E M, Zhang S and Zhang X 2020 *J. Magn. Magn. Mater.* **493** 165724
[63] Milde P, Köhler D, Seidel J, Eng L M, Bauer A, Chacon A, Kindervater J, Mühlbauer S, Pfleiderer C, Buhrandt S, Schütte C and Rosch A 2013 *Science* **340** 1076
[64] Oike H, Kikkawa A, Kanazawa N, Taguchi Y, Kawasaki M, Tokura Y and Kagawa F 2015 *Nat. Phys.* **12** 62